

## Effect of bond-disorder on the phase-separation kinetics of binary mixtures: A Monte Carlo simulation study

Awaneesh Singh, Amrita Singh, and Anirban Chakraborti

Citation: *The Journal of Chemical Physics* **147**, 124902 (2017); doi: 10.1063/1.5004563

View online: <http://dx.doi.org/10.1063/1.5004563>

View Table of Contents: <http://aip.scitation.org/toc/jcp/147/12>

Published by the [American Institute of Physics](#)

---

---



**Scilight**

Sharp, quick summaries **illuminating**  
the latest physics research

Sign up for **FREE!**

**AIP**  
Publishing

# Effect of bond-disorder on the phase-separation kinetics of binary mixtures: A Monte Carlo simulation study

Awaneesh Singh,<sup>1,2,a)</sup> Amrita Singh,<sup>2</sup> and Anirban Chakraborti<sup>2,b)</sup>

<sup>1</sup>Department of Physics, Institute of Chemical Technology, Mumbai 400019, India

<sup>2</sup>School of Computational and Integrative Sciences, Jawaharlal Nehru University, New Delhi 110067, India

(Received 30 April 2017; accepted 13 September 2017; published online 29 September 2017)

We present Monte Carlo (MC) simulation studies of phase separation in binary ( $AB$ ) mixtures with bond-disorder that is introduced in two different ways: (i) at randomly selected lattice sites and (ii) at regularly selected sites. The Ising model with spin exchange (Kawasaki) dynamics represents the segregation kinetics in conserved binary mixtures. We find that the dynamical scaling changes significantly by varying the number of disordered sites in the case where bond-disorder is introduced at the randomly selected sites. On the other hand, when we introduce the bond-disorder in a regular fashion, the system follows the dynamical scaling for the modest number of disordered sites. For a higher number of disordered sites, the evolution morphology illustrates a lamellar pattern formation. Our MC results are consistent with the Lifshitz-Slyozov power-law growth in all the cases. *Published by AIP Publishing.* <https://doi.org/10.1063/1.5004563>

## I. INTRODUCTION

A binary ( $AB$ ) mixture that is homogeneous (or disordered) at high temperatures becomes thermodynamically unstable when rapidly quenched inside the coexistence curve. Then, the binary ( $AB$ ) mixture undergoes phase separation (or ordering) via the formation and growth of domains enriched in either component. Much research interest has focused on this far-from-equilibrium evolution.<sup>1–6</sup> The domain morphologies are usually quantified by two important properties: (a) the domain growth law [characteristic domain size  $L(t)$  grows with time  $t$ ], which depends on general system properties, e.g., the nature of conservation laws governing the domain evolution, the presence of hydrodynamic velocity fields, the presence of quenched or annealed disorder, etc., and (b) the correlation function or its Fourier transform, the structure factor, which is a measure of the domain morphology.<sup>1,2</sup>

There now exists a good understanding of phase separation dynamics of  $AB$ -mixtures.<sup>7–12</sup> Normally, for a pure and isotropic system, domain growth follows a power-law behavior,  $L(t) \sim t^\phi$  where  $\phi$  is referred to as the growth exponent. For the case with a nonconserved order parameter (ordering of a magnet into up and down phases), the system obeys the Lifshitz-Cahn-Allen (LCA) growth law with  $\phi = 1/2$ .<sup>1–4</sup> For the case with a conserved order parameter (diffusion driven phase separation of an  $AB$  mixture into  $A$ -rich and  $B$ -rich phases), the system obeys the Lifshitz-Slyozov (LS) growth law with  $\phi = 1/3$ .<sup>1–4</sup> However, including the hydrodynamic effects in a system with a conserved order parameter (e.g., segregation of a binary fluid), there appear to be various domain growth regimes, depending on the dimensionality and system parameters.<sup>9,13–16</sup>

In reality, the experimental systems are neither pure nor isotropic. Usually, they always endure impurities (annealed or quenched) within the system. An important set of results has been well documented from both analytical and numerical studies on phase ordering in systems with quenched disorder.<sup>17–27</sup> The quenched disorder (considered as an immobile impurity) is introduced into the pure Ising model either by random spin-spin exchange interaction, i.e., random-bond Ising model (RBIM)<sup>20,26,27</sup> or introducing a site-dependent random-field Ising model (RFIM).<sup>28,29</sup> In general, sites of quenched disorder act as traps for domain boundaries with the energy barrier being dependent on the domain size. In this regard, a significant contribution is made by Huse and Henley (HH)<sup>17</sup> to understand the growth law for the bond-disorder case. They argued that the energy barrier follows power-law dependence on domain size:  $E_b(L) \simeq \epsilon L^\psi$ . Here,  $\epsilon$  is the disorder strength and  $\psi$  is the barrier exponent that depends on the roughening exponent  $\zeta$  and the pinning exponent  $\chi$  as  $\psi = \chi/(2 - \zeta)$ ; the roughening and pinning exponents are related as  $\chi = 2\zeta + d - 3$ , where  $d$  is the system dimensionality. Consequently, the normal power-law growth [ $L(t) \sim t^\phi$ ] of the characteristic domain size changes over to a logarithmic growth  $L(t) \sim (\ln t)^\phi$ . A few numerical simulations<sup>18–25,30</sup> and experiments<sup>31–33</sup> were performed to test the HH proposal. Nevertheless, to date, no definite confirmation of logarithmic growth in the asymptotic regime is observed.

Later, Paul, Puri, and Rieger (PPR)<sup>26,27</sup> reconsidered this problem via extensive Monte Carlo (MC) simulations of the RBIM with nonconserved (Glauber) spin-flip kinetics and conserved (Kawasaki) spin exchange kinetics. In contrast to the HH scenario, PPR observed the normal power-law domain growth with temperature and disorder dependent growth exponent, similar to the one seen in the experiments<sup>31–33</sup> on domain growth in the disordered system. PPR proposed that the growth exponents can be understood in the framework of a logarithmic domain size dependence of trapping barrier [ $E_b(L)$

<sup>a)</sup>awaneesh11@gmail.com

<sup>b)</sup>anirban@jnu.ac.in

$\approx \epsilon \ln(1 + L)$ ] rather than the power-law.<sup>26</sup> At early times, domain coarsening is not affected by disorder due to small energy barriers, and therefore, the system evolves like a pure system. At late times, the disorder traps become effective at a crossover length scale, and it can only move by thermal activation over the corresponding energy barrier. Thus, thermal fluctuations drive the asymptotic domain growth in disordered systems.<sup>26,27</sup> This should be contrasted with the pure case, where thermal fluctuations are irrelevant. In these cases, quench disorder was introduced by uniformly varying the strength of the spin-spin exchange interaction between zero and one at all the lattice sites.

In this paper, we present MC simulations of domain coarsening in binary mixtures with quenched disorder using conserved (Kawasaki) spin-exchange kinetics. Here, we introduce the disorder in two different ways: (a) at randomly selected lattice sites and (b) at regularly selected lattice sites. We consider the strength of the spin-spin exchange interaction equal to zero at these selected sites (equivalent to have sites at  $T \gg T_c$  called disordered sites) and equal to one at the rest of the sites. By varying the number of selected sites, we discuss the effect of disorder on the domain growth law and the dynamical scaling. Our simulations are aimed to gain a conceptual understanding of these disordered systems where theoretical calculations are challenging at present. This paper is organized as follows. In Sec. II, we describe the methodology we used to simulate the system. In Sec. III, we present the results and discussion for both the cases of introducing disorder. Finally, Sec. IV concludes this paper with the summary of our results.

## II. METHODOLOGY

Let us start with a description of Monte Carlo (MC) simulations for the study of phase separation in binary ( $AB$ ) mixtures. The Hamiltonian for the Ising system is described by

$$H = - \sum_{\langle ij \rangle} J_{ij} S_i S_j, \quad S_i = \pm 1. \quad (1)$$

Here,  $S_i$  denotes the spin variable at site  $i$ . We consider two state spins:  $S_i = +1$  when a lattice site  $i$  is occupied by an  $A$  atom and  $S_i = -1$  when occupied by a  $B$  atom. The subscript  $\langle ij \rangle$  in Eq. (1) denotes a sum over nearest-neighbor pairs only. The term  $J_{ij}$  denotes the strength of the spin-spin exchange interaction between nearest-neighbor spins. We consider the case where  $J_{ij} \geq 0$  so that the system is locally ferromagnetic. The case where a system has both  $J_{ij} \geq 0$  (ferromagnetic) and  $J_{ij} \leq 0$  (antiferromagnetic) is relevant to spin glasses. Normally, in MC simulations for a pure phase-separating binary ( $AB$ ) mixture, we consider  $J_{ij} = 1$  with a critical temperature  $T_c \approx 2.269/k_B$  for a  $d = 2$  square lattice. Further,  $J_{ij} = 0$  corresponds to the maximally disordered system, equivalent to the system at  $T \gg T_c$  where all proposed spin exchanges will be accepted.

In our MC simulations, spins are placed on a square lattice ( $L_x \times L_y$ ) with periodic boundary conditions in both the directions. We assign random initial orientations: up ( $S_i = +1$ ) or down ( $S_i = -1$ ) to each spin and rapidly quench the system to  $T < T_c$ . The quench disorder is introduced via exchange

coupling as  $J_{ij} = 1 - \epsilon$ , where  $\epsilon$  quantifies the degree of disorder. In this paper, we consider only two values of the degree of disorder,  $\epsilon = 0$  (pure system) and  $\epsilon = 1$  (disordered sites corresponding to impurities in the system). Notably, in PPR's study,<sup>26</sup>  $J_{ij}$  is uniformly distributed in the interval  $[1 - \epsilon, 1]$ , where the limit  $\epsilon = 0$  corresponds to the pure case and  $\epsilon = 1$  corresponds to the maximally disordered case with  $J_{ij} \in [0, 1]$ .

We perform our MC simulations for two different cases corresponding to the way we introduce disorder into the system. In case 1, we randomly select a fraction of sites with  $\epsilon = 1$ , and in case 2, we pick the same fraction of sites in a regular fashion. The remaining lattice sites are set to  $\epsilon = 0$ . Shortly, we present the results for three different percentages of disordered sites ( $\epsilon = 1$ ), namely, at 2%, 5%, and 10% of total sites,  $N$ , for both the cases and compare them with the pure case ( $\epsilon = 0$ ). The initial condition of the system corresponds to a critical quench with 50%  $A$  (up) and 50%  $B$  (down) spins.

We place the Ising system in contact with a heat bath to associate stochastic dynamics. The resultant dynamical model is referred to as a *kinetic Ising model*. We consider spin-exchange (Kawasaki) kinetics, an appropriate model to study the phase separation in  $AB$  mixtures.<sup>2,7</sup> It is straight forward to implement MC simulations of the Ising model with spin-exchange kinetics. In a single step of MC dynamics, a randomly selected spin  $S_i$  is exchanged with a randomly chosen nearest-neighbor  $S_j$  ( $S_i \leftrightarrow S_j$ ). The change in energy  $\Delta H$  that would occur if the spins were exchanged is computed. The step is then accepted or rejected with the Metropolis acceptance probability,<sup>34,35</sup>

$$P = \begin{cases} \exp(-\beta\Delta H) & \text{for } \Delta H \geq 0, \\ 1 & \text{for } \Delta H \leq 0. \end{cases} \quad (2)$$

Here,  $\beta = (k_B T)^{-1}$  denotes the inverse temperature and  $k_B$  is the Boltzmann constant. One Monte Carlo step (MCS) is completed when this algorithm is performed  $N$  times (where  $N$  is the total number of spins), regardless of whether the move is accepted or rejected. Noticeably, if at least one of the spin in the randomly chosen spin pair belongs to the disordered site, the proposed spin exchange will be accepted.

The morphology of the evolving system is usually characterized by studying the two-point ( $\vec{r} = \vec{r}_1 - \vec{r}_2$ ) equal-time correlation function,

$$C(\vec{r}, t) = \frac{1}{N} \sum_{i=1} [\langle S_i(t) S_{i+\vec{r}}(t) \rangle - \langle S_i(t) \rangle \langle S_{i+\vec{r}}(t) \rangle], \quad (3)$$

which measures the overlap of the spin configuration at distance ( $\vec{r}$ ). Here, the angular brackets denote an average over different initial configurations and different noise realizations. However, most experiments study the structure factor, which is the Fourier transform of the correlation function,

$$S(\vec{k}, t) = \sum_{\vec{r}} \exp(i\vec{k} \cdot \vec{r}) C(\vec{r}, t), \quad (4)$$

where  $\vec{k}$  is the scattering wave-vector. Since the system under consideration is isotropic, we can improve statistics by spherically averaging the correlation function and the structure factor. The corresponding quantities are denoted as

$C(r, t)$  and  $S(k, t)$ , respectively, where  $r$  is the separation between two spatial points and  $k$  is the magnitude of the wave-vector.

It is now a well-established fact that the domain coarsening during phase separation is a scaling phenomenon. The correlation function and the structure factor exhibit the dynamical scaling form<sup>1,2</sup>

$$C(r, t) = g[r/L(t)], \quad (5)$$

$$S(k, t) = L(t)^d f[kL(t)]. \quad (6)$$

Here,  $g(x)$  and  $f(p)$  are the scaling functions. The characteristic length scale  $L(t)$  (in the units of lattice spacing) is defined from the correlation function as the distance over which it decays to (say) zero or any fraction of its maximum value [ $C(r = 0, t) = 1$ ]; we find that the decay of  $C(r, t)$  to 0.1 gives a good measure of average domain size  $L(t)$ . There are few different definitions of the length scale, but all these are equivalent in the scaling regime, i.e., they differ only by constant multiplicative factors.<sup>7,36</sup>

### III. NUMERICAL RESULTS

Using our MC simulations, we present results for the structure and dynamics of a phase separating symmetric binary mixture (50%A and 50%B) with the bond-disorder. We discuss both the cases of introducing the disorder (case 1: at randomly selected sites and case 2: at regularly selected sites). The simulations are performed on a system of  $N = L_x \times L_y$  particles of type A and B confined to a square lattice ( $d = 2$ ,  $L_x = L_y = 512$ ) such that the number density  $\rho = 1.0$ . We quench the system from a high-temperature homogeneous phase to a temperature  $T = 1.0$  ( $T < T_c$ ) and then monitor the evolution of the system at various Monte Carlo steps. In presenting these results, our purpose is two-fold: first, we analyze the effects of bond-disorder on domain coarsening and how the number of disordered sites ( $N_1$ ) influences the characteristic features of the domain morphologies and scaling behavior. Second, we intend to study how the different ways of introducing the same disorder affect phase separating kinetics in the system.

#### A. Disorder at randomly selected sites

We present evolution morphologies of AB mixtures obtained from our MC simulations for case 1 in Fig. 1 at  $t = 4 \times 10^5$  and  $t = 1.6 \times 10^6$  MCS. Figure 1 displays the evolution pictures for four different percentages of disordered sites: (a) 0% ( $N_1 = 0$ ; pure case), (b) 2% ( $N_1 = N/50$ ), (c) 5% ( $N_1 = N/20$ ), and (d) 10% ( $N_1 = N/10$ ), respectively. Immediately after the quench, the system starts evolving via the emergence and growth of domains, namely, A-rich (marked in blue) and B-rich (unmarked) regions. As expected, for a symmetric (critical) composition, a bicontinuous domain structure is seen for the pure case [Fig. 1(a)]. Whereas, with the increase of disordered sites ( $N_1$ ), roughening of domain walls increases<sup>17</sup> due to the fact that at the disordered sites all the proposed spin exchanges are accepted, and hence, domains look more fuzzier with increasing  $N_1$ .

To study the domain morphology, we plot the scaled correlation function [ $C(r, t)$  vs.  $r/L(t)$ ] in Fig. 2(a) at three different

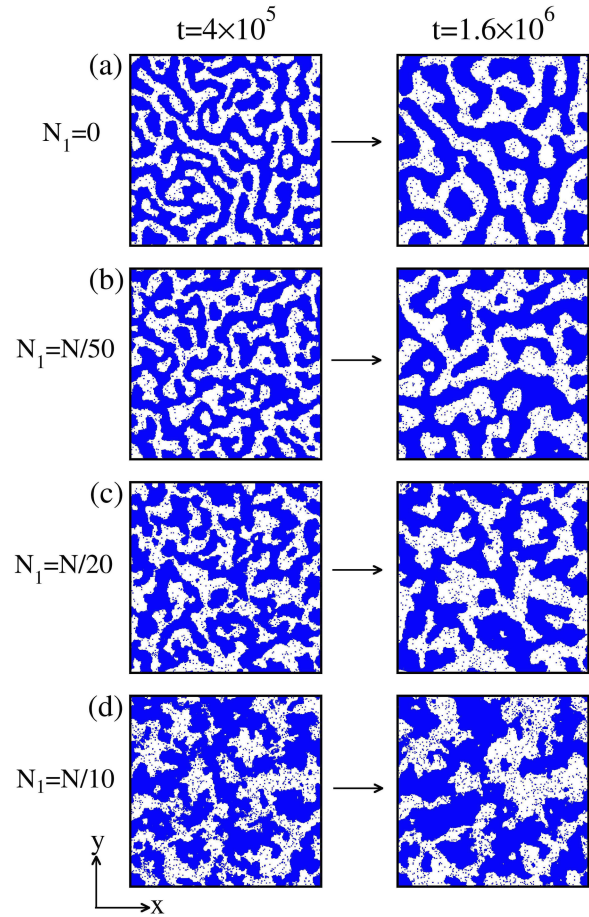


FIG. 1. Snapshots at  $t = 4 \times 10^5$  and  $t = 1.6 \times 10^6$  MCS, exhibiting the domain coarsening for four different percentages of disordered sites (a) 0% ( $N_1 = 0$ ; pure case), (b) 2% ( $N_1 = N/50$ ), (c) 5% ( $N_1 = N/20$ ), and (d) 10% ( $N_1 = N/10$ ). The disorder is introduced at randomly selected sites. The numerical details of the simulations are described in the text.

times during the evolution. Here, we considered case 1 with 5% of disordered sites [see Fig. 1(c)];  $L(t)$  is defined as the distance over which  $C(r, t)$  decays to 0.1 of its maximum value [ $C(0, t) = 1$ ]. A neat data collapse demonstrates the dynamical scaling of the domain morphologies and confirms that the system for a given  $N_1$  belongs to the same dynamical universality class. An excellent data collapse of the structure factor [a log-log plot of

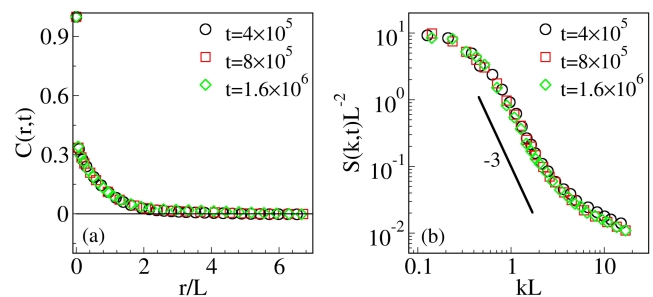


FIG. 2. (a) Scaling plot of  $C(r, t)$  vs.  $r/L$  when 5% of randomly selected disordered sites are present in the system. The data sets at  $t = 4 \times 10^5$ ,  $t = 8 \times 10^5$ , and  $t = 1.6 \times 10^6$  MCS collapse nicely onto a single curve. (b) Plot of  $S(k, t)L^{-2}$  vs.  $kL$  corresponding to the same data sets as in (a). The large  $k$  region (tail) of the structure factor deviates from Porod's law,  $S(k, t) \sim k^{-3}$  for  $k \rightarrow \infty$ . The correlation function and the structure factor data sets are obtained as an average over ten independent runs.

$S(k, t)L^{-2}$  vs.  $kL$  in Fig. 2(b)], obtained from the Fourier transform of the correlation function data sets presented in Fig. 2(a), also demonstrates the dynamical scaling. However, for large  $k$  values,  $S(k, t)$  deviates from the well-known Porod's law,  $S(k, t) \sim k^{-(d+1)}$ , which results from scattering off sharp interfaces.<sup>37,38</sup> For other values of  $N_1$ , the correlation function and the structure factor exhibit the similar scaling behavior (not shown here).

We now discuss how the evolution morphology depends on the number of disordered sites,  $N_1$ . Figure 3(a) shows the scaled correlation function for three different values of  $N_1$  at  $t = 1.6 \times 10^6$  MCS when the system is already in the scaling regime (see the evolution snapshots in Fig. 1). The scaled correlation function for a pure binary mixture (denoted by the black symbols) is also included as a reference. Our results suggest that the data sets do not collapse onto a master function; therefore, the system does not belong to the same dynamical universality class. Thus, the scaling functions clearly depend upon the number of disordered sites,  $N_1$ .

In Fig. 3(b), we present the scaling plot of the structure factor,  $S(k, t)L^{-2}$  vs.  $kL$  on a log-log scale, corresponding to the data sets in Fig. 3(a). For the pure system, the structure factor tail obeys Porod's law,  $S(k, t) \sim k^{-(d+1)}$  (indicated by the black symbols) as there are large regions of pure phases separated by sharp interfaces.<sup>37,38</sup> A black solid line shows the slope ( $-3$ ) of the structure factor tail. The structure factor data at three different values of  $N_1 = 2\%$ ,  $5\%$ , and  $10\%$  are demonstrated by the red, green, and blue curves, respectively. Corresponding slopes of the structure factor tail are  $-2.2$  (red dashed line),  $-0.92$  (green dashed line), and  $-0.48$  (blue dashed line), respectively.

A deviation of the structure factor tail from Porod's law to a lower noninteger exponent suggests a non-Porod behavior [i.e.,  $S(k, t) \sim k^{-(d+\theta)}$ , with  $\theta < 1$ ].<sup>39-41</sup> This is due to the presence of fractal architecture in the domains or interfaces as a consequence of interfacial roughening caused by quenched disorder. At a higher number of disordered sites, the exponent values are less than 2 ( $d + \theta \approx 0.92$  for  $N_1 = N/20$  and  $0.48$  for  $N_1 = N/10$ ) which suggest that the corresponding morphologies are *mass fractals* with fractal dimension  $d_f \approx d + \theta$ .<sup>39,40</sup>

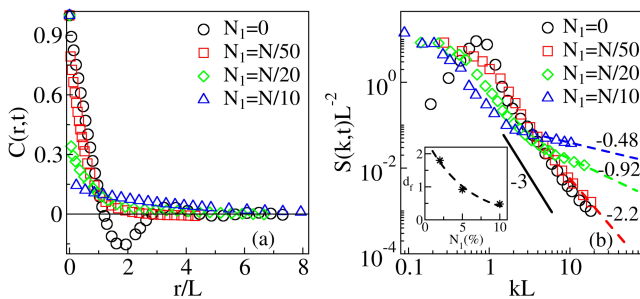


FIG. 3. (a) Plot of  $C(r, t)$  vs.  $r/L$  (for the evolution shown in Fig. 1 at  $t = 1.6 \times 10^6$  MCS) at four different values of  $N_1$  as denoted by the specified symbol type. With increasing  $N_1$ , data sets gradually deviate from the pure case (black curve). (b) Plot of  $S(k, t)L^{-2}$  vs.  $kL$  corresponding to the data sets in (a). For the pure case, the structure factor curve follows Porod's law [ $S(k, t) \sim k^{-3}$  for  $k \rightarrow \infty$ ]. With increased disordered sites, there is a clear deviation of the tail to non-Porod's law described in the text. The inset shows the variation of  $d_f$  with  $N_1$ .

On the other hand, for  $N_1 = N/50$ ,  $(d + \theta) \approx 2.2 > 2$  indicates a rough morphology with a surface fractal dimension  $d_f \approx d - \theta = 1.8$ .<sup>39-41</sup> The inset of Fig. 3(b) demonstrates the decrease of fractal dimension,  $d_f$ , under the influence of the number of disordered sites  $N_1$ . Notice that the structure factor peak shifted to lower  $k$  values with increasing  $N_1$ , which corresponds to a large-scale structure in the system which is evident in Fig. 1(d). This further confirms the  $N_1$  dependent scaling functions.

The results of the time dependence of average domain size  $L(t)$  vs.  $t$  are displayed in Fig. 4 for the morphologies shown in Fig. 1. For the pure case ( $\epsilon = 0$ ), coarsening morphology follows the standard Lifshitz-Slyozov (LS) growth law:  $L(t) \sim t^{1/3}$  (black symbols); the black solid line represents the expected growth exponent ( $\phi = 1/3$ ) in Fig. 4(a). For all values of  $N_1 \neq 0$ , our data clearly follow the LS growth law for an extended period, although the prefactors of the power-law growth vary with  $N_1$ . However, on the time scale of our simulation, the domain growth law for  $N_1 = 10\%$  crosses over to the saturation beyond  $t > 10^6$ , which is a sign of the presence of frozen morphologies due to the presence of fractal structures which causes the localization of diffusive particles.<sup>39</sup>

Another concurrent way of extracting the growth exponent is to calculate an instantaneous growth exponent,<sup>41-45</sup>

$$\phi_i = \frac{d \ln L(t)}{d \ln t}. \quad (7)$$

The corresponding plots of  $\phi_i$  as a function of  $1/L(t)$  are shown in Fig. 4(b). Notice that at late times as domain size increases,  $\phi_i$  fluctuates around the asymptotic growth exponent value,  $1/3$  (black solid line), hence our data is consistent with the LS growth law. We notice a slightly lower growth exponent in the pure case at few early times ( $t = 4000 - 16\,000$  MCS). The value of  $\phi_i$ , usually much less than  $1/3$ , is due to the transient evolution regime appears at early times of phase ordering. However, in our case, we collect data for  $1.6 \times 10^6$  MCS at an interval of 4000 MCS. We observe that by 4000 MCS, the transient coarsening regime begins to enter the scaling regime, and hence, we do not observe the much lower values of  $\phi_i$ .<sup>41,44,45</sup>

Overall, we find that the system with the disorder at randomly selected sites follows the expected LS power-law

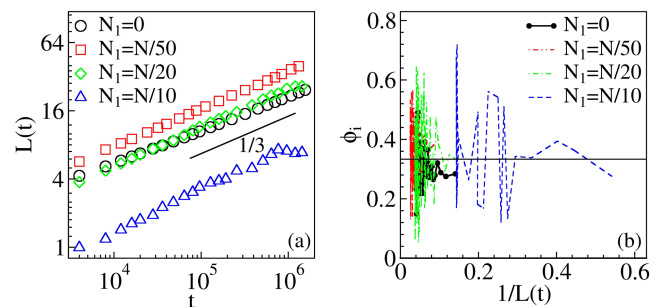


FIG. 4. (a) Log-log plot of the time dependence of the characteristic length scale for the evolution shown in Fig. 1. The symbol types represent different percentages of disordered sites. The solid black line shows the expected growth exponent  $\phi = 1/3$  for the pure binary mixture. (b) Variation of instantaneous growth exponent  $\phi_i$  as a function of  $1/L(t)$  for the data shown in (a).

growth:  $L(t) \sim t^\phi$  with  $\phi = 1/3$ .<sup>46</sup> For a fixed number of disordered sites ( $N_1$ ), the system displays the dynamical scaling at various time steps. However, the system deviates significantly from the dynamical scaling for different  $N_1$  values at a fixed time step.

## B. Disorder at regularly selected sites

We now examine case 2, where the disorder is introduced at regularly selected sites by keeping the other numerical details same as in case 1. The entire system consists of  $N = L_x \times L_y$  sites. The set of indices  $i = 1 \dots L_x$  and  $j = 1 \dots L_y$  defines the respective positions of the sites in  $x$  and  $y$  directions. We sweep the entire lattice sites ( $N$ ) by tracing all the indices in the  $y$ -direction ( $1 \dots L_y$ ) at each fixed  $i$ . In the process, every  $m$ th site is selected to introduce the quench disorder. The total number of disordered sites in the system are  $N_1 = N/m$ . We investigate the domain morphologies and the corresponding scaling properties by varying the number of disordered sites ( $N_1$ ) and compare them with the pure case ( $\epsilon = 0$ ) as described for case 1.

Figure 5 shows the evolution morphologies at  $t = 4 \times 10^5$  and  $t = 1.6 \times 10^6$  MCS for the number of disordered sites (a)  $N_1 = 0$  (0%), (b)  $N_1 = N/50$  (2%), (c)  $N_1 = N/20$  (5%), and (d)  $N_1 = N/10$  (10%), respectively. After the temperature quench,  $A$ -rich (marked in blue) and  $B$ -rich (unmarked) domains start

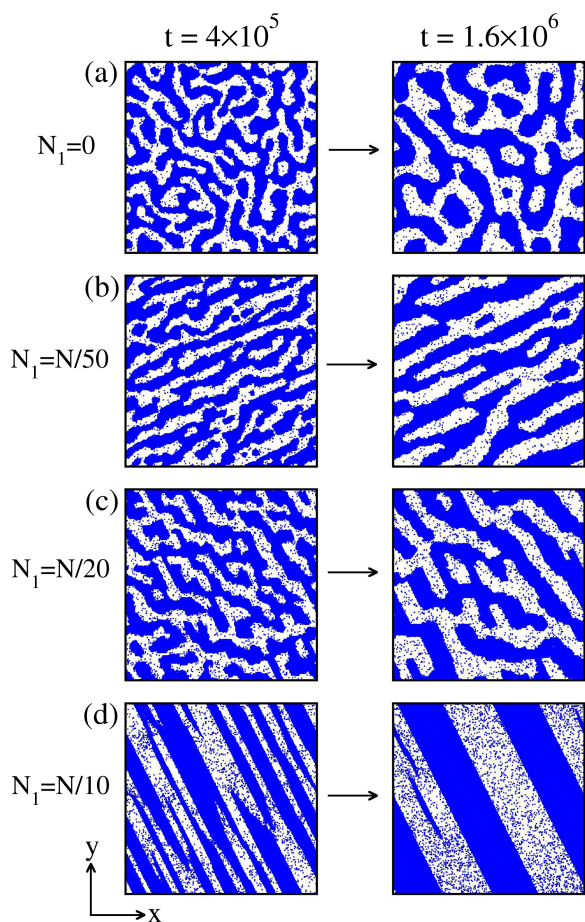


FIG. 5. Snapshots at  $t = 4 \times 10^5$  and  $t = 1.6 \times 10^6$  MCS, for various percentages of disordered sites in the system ( $N_1$ ): (a) 0%, (b) 2%, (c) 5%, and (d) 10%. The disorder is introduced at regularly selected sites. Other numerical details of the simulations are described in the text.

growing with the passage of time. In this process, where we select disordered sites in a regular manner, stripe patterns are observed [see Figs. 5(b)–5(d)]. In Fig. 5(d), we find that with  $N_1 = 10\%$ , the evolution of a striped pattern resulting in a lamellar pattern at late times. Furthermore, we believe that even with a lower number of disordered sites ( $N_1 = 2\%$  and  $5\%$ ), lamellar patterns could be observed at late times  $t \gg 1.6 \times 10^6$  MCS [see Figs. 5(b) and 5(c)], whereas such lamellar patterns occurred earlier for  $N_1 = 10\%$ .

Recall that we consider  $J = 0$  (i.e.,  $T \gg T_c$ ) at the disordered sites and therefore accept all proposed spin exchanges with the nearest-neighbor spins at these locations. Evidently, after the quench, phase separation also begins due to the exchange of spins at neighboring sites. Therefore, to start the spin-exchange dynamics, most favorable locations would be the neighborhoods of the given disordered sites. Hence, we start noticing the formation of clusters along the disordered sites at early times that leads the system to display lamellar patterns at late times. To validate above points, we further performed a few separate experiments, where the disorder was introduced in various regular manners (not shown here). Each time we observed that the growth of domains started along the disordered sites that later formed the striped/lamellar patterns aligned along the direction of the disordered sites. Figures 5(b)–5(d) also reveal the dependence of stripe orientation on the number of disordered sites,  $N_1$ . Thus, by the combination of phase separation phenomenon of a binary mixture and the introduction of disorder at the regularly selected sites, one can guide the typical morphology of the coexisting  $A$  and  $B$  phases into an ordered striped/lamellar pattern.

Next, we present the scaling plots of the correlation function [ $C(r, t)$  vs.  $r/L(t)$  in Fig. 6(a)] and the structure factor [ $S(k, t)L^{-2}$  vs.  $kL$  in Fig. 6(b)], defined in Eq. (5). Figure 6 corresponds to the morphologies shown in Fig. 5(c) with 5% disordered sites. We plot the scaling functions at three time instants as indicated by the symbols. The dynamics regarding the correlation function and the structure factor at different times has shown a perfect congruence with each other witnessing the universality in their behavior as well as confirming the validity of dynamical scaling. We also observed that unlike the previous case, here the structure factor data obeys Porod's

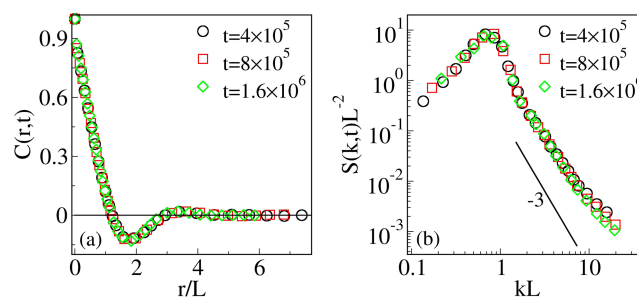


FIG. 6. (a) Scaling plot of  $C(r, t)$  vs.  $r/L$  with  $N_1 = 5\%$  at regularly selected sites. The data sets at  $t = 4 \times 10^5$ ,  $t = 8 \times 10^5$ , and  $t = 1.6 \times 10^6$  MCS collapse nicely onto a single curve. (b) Scaling plot of  $S(k, t)L^{-2}$  vs.  $kL$  corresponding to the same data sets as in (a). The structure factor tail (large  $k$  region) obeys Porod's law  $S(k, t) \sim k^{-3}$  for  $k \rightarrow \infty$  for all the values of  $N_1$  as represented by specified symbols.

law [ $S(k, t) \sim k^{-3}$  as  $k \rightarrow \infty$ ] which results from scattering off sharp interfaces.

We now discuss whether the evolution morphology depends on the number of disordered sites present in the system. Figures 7(a) and 7(b) show a comparison of the scaled correlation function and the corresponding structure factor at four different percentages of disordered sites ( $N_1 = 0\%$ , 2%, 5%, and 10%) for  $t = 1.6 \times 10^6$  MCS. At lower values of  $N_1$ , particularly at 2% and 5%, excellent data collapse with the pure case ( $N_1 = 0\%$ ) suggests that they belong to the same dynamical universality class, i.e., the morphologies are equivalent and their statistical properties are independent of  $N_1$ . However, for  $N_1 = 10\%$ , the interconnected morphology of A and B phases transformed into an ordered lamellar pattern,

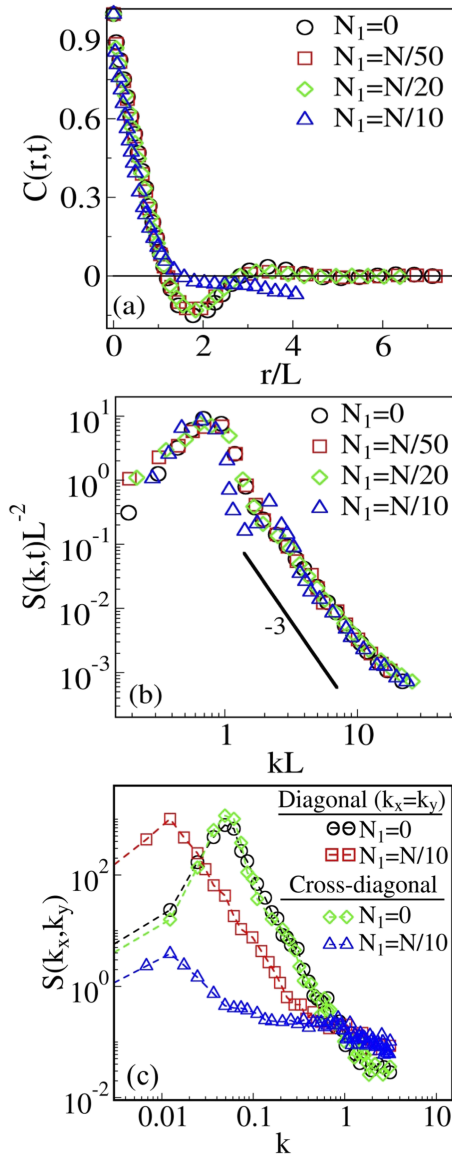


FIG. 7. (a) Plot of  $C(r, t)$  vs.  $r/L$  for the evolutions shown in Fig. 5 at  $t = 1.6 \times 10^6$ . Except at  $N_1 = 10\%$ , we observe a good data collapse for other percentages of disordered sites (0%, 2% and 5%). (b) Plot of  $S(k, t)L^{-2}$  vs.  $kL$  corresponding to the data sets in (a). For all the cases, the tail of the structure factor obeys Porod's law  $S(k, t) \sim k^{-3}$  for  $k \rightarrow \infty$ . The correlation function and the structure factor data sets are obtained as an average over ten independent runs. (c) Plot of  $S(k_x, k_y)$  along the lattice diagonals for the lamellar and pure cases.

hence the deviation from the dynamical scaling. Notice that the scaled correlation function for  $N_1 = 10\%$  (shown by the blue symbols) in Fig. 7(a) exhibits a crossover due to the formation of lamellar morphology. In Fig. 7(b), the structure factor data sets also manifest the excellent data collapse on the master curve for  $N_1 = 0\%$ , 2%, 5%. However, notice that the structure factor shows a distinct shoulder for  $N_1 = 10\%$ , which characterizes the lamellar structure in Fig. 5(d). The scaled structure factor shows a Porod tail  $S(k, t) \sim k^{-(d+1)}$  as  $k \rightarrow \infty$  for all the values  $N_1$ .

It is well known that the domain structure of a system is visible from the higher-order Bragg-reflections in  $S(\vec{k}, t)$ , namely, at  $(2n + 1)k_m$  for  $n = 1, 2, \dots$ . The scattering around  $k_m$  dominates the  $S(\vec{k}, t)$  spectrum and leads to a narrow peak. Since we are working in a finite lattice, only a discrete set of  $k$ -vectors is physically meaningful:  $\vec{k} = (2\pi\vec{n}/L)$  with  $\vec{n} = (n_x, n_y)$  where  $0 \leq n_i \leq L$  for  $i = x, y$ .<sup>47</sup> The ordered phase is then detected by the number of peaks in the structure factor,  $S(\vec{k}, t)$ , produced by the periodicity of the morphology for all these  $k$ -vectors. For simplicity, we generally looked at the spherically averaged structure factor,  $S(k, t)$ , even in the lamellar case, as our main aim was to probe the periodicity induced due to the formation of lamellar morphologies [see the second peak in Fig. 7(b)].

Further, to explore the anisotropy introduced in the system due to stripes [Fig. 5(d),  $N_1 = N/10$ ], we calculate  $S(k_x, k_y)$  normal (along the diagonal of lattice) and parallel (along the cross-diagonal) to the lamellar as depicted in Fig. 7(c). We observe that the structure factor, normal to the stripe, retains a sharp and high amplitude peak (red curve). On the other hand, the peak strength of the structure factor, along the stripe, remains extremely low (blue curve). Both the curves [red and blue in Fig. 7(c)] clearly suggest the presence of anisotropy in the system. For comparison, we also plot  $S(k_x, k_y)$  for the pure case ( $N_1 = 0$ ). The black and green curves in Fig. 7(c) represent  $S(k_x, k_y)$  along the diagonal and cross-diagonal of the lattice, respectively. The excellent overlap of both the curves suggests the structural isotropy in the pure system. Notice that we do not present the usual scaling plot in Fig. 7(c), where data sets at different times collapse onto a master function.

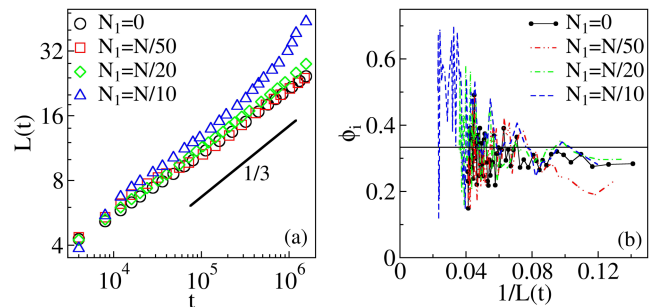


FIG. 8. (a) Log-log plot of the time dependence of the characteristic length scale for the evolution shown in Fig. 5. The symbol types represent the number of disordered sites. The line of slope  $1/3$  corresponds to the expected growth regime for the pure binary mixture. (b) Variation of instantaneous growth exponent  $\phi$  vs.  $1/L(t)$  for the data shown in (a). Solid line marks the average value of  $1/3$ .

Finally, we turn our attention to the time dependence of the domain size for the evolution shown in Fig. 5. We plot  $L(t)$  vs.  $t$  on a log-log scale in Fig. 8(a) for various  $N_1$  values. The corresponding plots of  $\phi_i$  vs.  $1/L(t)$  are shown in Fig. 8(b). Our results clearly indicate a convergence to  $\phi = 1/3$  for  $L(t) \rightarrow \infty$ , at the lower percentages of disorder introduced at regularly selected sites. However, at a higher number of disordered sites, we observe the presence of more fuzziest clusters, which indicate that the diffusive dynamics (where the average displacement of a particle is proportional to  $t^{1/2}$ ) effectively sets in with phase separation kinetics. Hence, we observed a gradual crossover of the growth exponent from  $1/3$  to  $1/2$  at late times. The slight upward trend of the curves for  $N_1 \neq 0$  in the log-log plot suggests that the growth cannot be slower than a power-law growth.

#### IV. CONCLUSIONS

We have performed extensive Monte Carlo simulations to study the segregation kinetics in binary mixtures with bond-disorder. Our studies are based on the kinetic Ising model with conserved (Kawasaki) spin-exchange dynamics. We have presented results for two different cases of bond-disorder in the system: (i) at randomly selected sites and (ii) at regularly selected sites, where the exchange interaction  $J = 1 - \epsilon$  with  $\epsilon = 1$  and remaining sites have  $\epsilon = 0$ . We have discussed the characteristic features of domain morphologies of phase separating (AB) mixtures with critical composition (50% A and 50% B) for a broad range of percentages of the disordered sites  $N_1 = 0\%$ , 2%, 5%, and 10%.

When the disorder was incorporated at randomly selected sites (case 1), the scaling functions  $C(r, t)$  and  $S(k, t)$  appeared to be dependent on the number of disordered sites. We observed that the domain growth law was always consistent with the Lifshitz-Slyozov (LS) growth law. However, on the time scale of our simulation, the data for a higher number of disordered sites (10%) have crossed over to a saturation regime. We have not accessed this crossover regime for lower percentages of disordered sites; nevertheless, we cannot rule out the possibility of saturation of the growth law at even later times than those investigated here.

Next, in case 2, where we introduced disorder at sites selected in a regular manner, evolution morphologies led to a stripped/lamellar pattern formation. In this case, for the lower percentages (2% and 5%) of disordered sites, domains morphologies, which were mostly connected stripes, showed a good scaling behavior. Whereas for 10% disordered sites, the system did not fall into the same universality class as the morphology was a lamellar pattern. Hence, we observed a corresponding crossover in the scaling functions. The domain growth law, in this case, was also consistent with the LS growth law on the time scale of our simulation as in case 1.

There are a number of physical systems where our model can be incorporated to understand the physical phenomena, for example, in self-organized pattern formation in ecological systems such as self-organizing mussel beds and bird feather color patterns due to phase separated nanostructures. In general, disordered systems are of significant and technological interests. Our model can be used to explain phase-separation

in multiphase fluid flows, mineral exsolution, and growth and structural transition in biological systems.

Finally, our simulations were performed for  $d = 2$ . For  $d = 3$ , we would expect to observe similar patterns during the evolution of the system for the case where the disorder is introduced at randomly selected sites. For case 2 where we systematically put the disorder, the growth pattern should depend on the number of disordered sites and the type of periodicity introduced in different layers. We would expect to have the lamellar pattern in that case also, particularly for the high number of disordered sites, but the orientation of the stripes in one portion of the system may differ from that in the other layers. In a future study, we will address these aspects for  $d = 3$  systems, where comparable experiments have not yet been performed. Hence, our simulations certainly provide important guidelines for future studies.

#### ACKNOWLEDGMENTS

A.S. is thankful to Professor Sanjay Puri, SPS, JNU, India for the fruitful discussion and providing the computational facilities. A.S. is grateful to CSIR, New Delhi for the financial support. A.C. acknowledges the financial support from Grant No. BT/BI/03/004/2003(C) of Government of India Ministry of Science and Technology, Department of Biotechnology, Bioinformatics division, and DST-PURSE grant given to JNU by the Department of Science and Technology, Government of India.

<sup>1</sup>A. J. Bray, *Adv. Phys.* **43**, 357–459 (1994).

<sup>2</sup>*Kinetics of Phase Transitions*, edited by S. Puri and V. Wadhawan (CRC Press, Boca Raton, FL, 2009).

<sup>3</sup>K. Binder and P. Fratzl, in *Materials Science and Technology* (Wiley-VCH Verlag GmbH & Co. KGaA, Weinheim, Germany, 2013).

<sup>4</sup>A. Onuki, *Phase Transition Dynamics* (Cambridge University Press, Cambridge, 2002).

<sup>5</sup>S. Dattagupta and S. Puri, *Dissipative Phenomena in Condensed Matter: Some Applications* (Springer Berlin Heidelberg, Berlin, 2004).

<sup>6</sup>R. A. L. Jones, *Soft Condensed Matter* (Oxford University Press, Oxford, 2008).

<sup>7</sup>A. Singh, A. Mukherjee, H. M. Vermeulen, G. T. Barkema, and S. Puri, *J. Chem. Phys.* **134**, 044910 (2011).

<sup>8</sup>A. Singh, S. Puri, and C. Dasgupta, *J. Chem. Phys. B* **116**, 4519–4523 (2012).

<sup>9</sup>A. Singh, S. Puri, and C. Dasgupta, *J. Chem. Phys.* **140**, 244906 (2014).

<sup>10</sup>A. Singh, R. Krishnan, and S. Puri, *Europhys. Lett.* **109**, 26006 (2015).

<sup>11</sup>S. K. Das, S. Puri, J. Horbach, and K. Binder, *Phys. Rev. E* **72**, 061603 (2005).

<sup>12</sup>S. K. Das, S. Puri, J. Horbach, and K. Binder, *Phys. Rev. Lett.* **96**, 016107 (2006).

<sup>13</sup>T. Koga and K. Kawasaki, *Phys. Rev. A* **44**, R817–R820 (1991).

<sup>14</sup>S. Puri and B. Dunweg, *Phys. Rev. A* **45**, R6977–R6980 (1992).

<sup>15</sup>S. Ahmad, S. K. Das, and S. Puri, *Phys. Rev. E* **85**, 031140 (2012).

<sup>16</sup>V. M. Kendon, J. C. Desplat, P. Bladon, and M. E. Cates, *Phys. Rev. Lett.* **83**, 576–579 (1999).

<sup>17</sup>D. A. Huse and C. L. Henley, *Phys. Rev. Lett.* **54**, 2708–2711 (1985).

<sup>18</sup>G. S. Grest and D. J. Srolovitz, *Phys. Rev. B* **32**, 3014–3020 (1985).

<sup>19</sup>D. J. Srolovitz and G. S. Grest, *Phys. Rev. B* **32**, 3021–3025 (1985).

<sup>20</sup>J. H. Oh and D. I. Choi, *Phys. Rev. B* **33**, 3448–3452 (1986).

<sup>21</sup>D. Chowdhury, M. Grant, and J. D. Gunton, *Phys. Rev. B* **35**, 6792–6795 (1987).

<sup>22</sup>S. Puri, D. Chowdhury, and N. Parekh, *J. Phys. A: Math. Gen.* **24**, L1087–L1097 (1991).

<sup>23</sup>S. Puri and N. Parekh, *J. Phys. A: Math. Gen.* **25**, 4127–4137 (1992).

<sup>24</sup>H. Hayakawa, *J. Phys. Soc. Jpn.* **60**, 2492–2495 (1991).

<sup>25</sup>A. J. Bray and K. Humayun, *J. Phys. A: Math. Gen.* **24**, L1185–L1191 (1991).

- <sup>26</sup>R. Paul, S. Puri, and H. Rieger, *Phys. Rev. E* **71**, 061109 (2005).
- <sup>27</sup>R. Paul, S. Puri, and H. Rieger, *Europhys. Lett.* **68**, 881–887 (2004).
- <sup>28</sup>T. Nattermann and J. Villain, *Phase Transitions* **11**, 5–51 (1988).
- <sup>29</sup>A. J. Bray and M. A. Moore, *J. Phys. C: Solid State Phys.* **18**, L927–L933 (1985).
- <sup>30</sup>M. F. Gyure, S. T. Harrington, R. Strilka, and H. E. Stanley, *Phys. Rev. E* **52**, 4632–4639 (1995).
- <sup>31</sup>H. Ikeda, Y. Endoh, and S. Itoh, *Phys. Rev. Lett.* **64**, 1266–1269 (1990).
- <sup>32</sup>V. Likodimos, M. Labardi, and M. Allegrini, *Phys. Rev. B* **61**, 14440–14447 (2000).
- <sup>33</sup>V. Likodimos, M. Labardi, X. K. Orlik, L. Pardi, M. Allegrini, S. Emonin, and O. Marti, *Phys. Rev. B* **63**, 064104 (2001).
- <sup>34</sup>K. Binder and D. W. Heermann, *Monte Carlo Simulations in Statistical Physics: An Introduction* (Springer-Verlag, Berlin, 1988).
- <sup>35</sup>M. E. J. Newman and G. T. Barkema, *Monte Carlo Methods in Statistical Physics* (Oxford University Press, Oxford, 1999).
- <sup>36</sup>Y. Oono and S. Puri, *Phys. Rev. Lett.* **58**, 836 (1987).
- <sup>37</sup>G. Porod, in *Small-Angle X-Ray Scattering*, edited by O. Glatter and O. Kratky (Academic Press, New York, 1982).
- <sup>38</sup>Y. Oono and S. Puri, *Mod. Phys. Lett. B* **2**, 861 (1988).
- <sup>39</sup>A. Bhupaty, R. Verma, V. Banerjee, and S. Puri, *J. Phys. Chem. Solids* **103**, 33–39 (2017).
- <sup>40</sup>G. P. Shrivastav, M. Kumar, V. Banerjee, and S. Puri, *Phys. Rev. E* **90**, 032140 (2014).
- <sup>41</sup>S. Ahmad, S. Puri, and S. K. Das, *Phys. Rev. E* **90**, 040302(R) (2014).
- <sup>42</sup>D. A. Huse, *Phys. Rev. B* **34**, 7845–7850 (1986).
- <sup>43</sup>A. Chakraborti, R. Toral, and J. D. Gunton, *Phys. Rev. B* **39**, 4386–4394 (1989).
- <sup>44</sup>S. Majumdar and S. K. Das, *Phys. Rev. E* **81**, 050102 (2010).
- <sup>45</sup>S. Majumdar and S. K. Das, *Phys. Chem. Chem. Phys.* **15**, 13209–13218 (2013).
- <sup>46</sup>S. K. Das and S. Puri, *Phys. Rev. E* **65**, 026141 (2002).
- <sup>47</sup>A. Hoffmann, J. Sommer, and A. Blumen, *J. Chem. Phys.* **106**, 6709 (1997).